International Journal of Steel Structures 17(2): 413-425 (2017)
DOI 10.1007/s13296-017-6004-x
ISSN 1598-2351 (Print)
ISSN 2093-6311 (Online)

International Journal of
STEEL
STRUCTURES
www.springer.com/journal/13296

Seismic Performance of Reduced Web Section Moment Connections

Seyedbabak Momenzadeh[1,*], Mohammad Taghi Kazemi[2], and Masoud Hoseinzadeh Asl[3]

[1]*Ph.D. Candidate, Department of Civil, Construction and Environmental Engineering, Iowa State University, IA, USA, 50011*
[2]*Associate Professor, Department of Civil Engineering, Sharif University of Technology, Tehran, P.O. Box:11155-9313, Iran*
[3]*Assistant Professor, Department of Civil Engineering, Tabriz University, Tabriz, P.O. Box: 51666-14766, Iran*

Abstract

Seismic behavior of beam-to-column connections can be improved by shifting the location of inelasticity away from the column's face. Such connections can be achieved by reducing the flange area at a specific distance from the beam-column connection, called reduced beam section (RBS), or by reducing web area by introducing a perforation into the web, called reduced web section (RWS). This paper presents a parametric study that is carried out on the effect of the perforation size, perforation location, and the beam span length in the RWS connections, using finite element modeling. Next, an interaction formula is derived for design purposes, and a step by step design method is developed. Finally, a frame is analyzed to verify the reliability of the proposed design process and assess the impact of the RWS connections on the behavior of special moment frames. The study concludes that RWS connections can effectively improve seismic performance of special moment frames, causing plastic hinges to form around the perforation away from the column's face.

Keywords: reduced web section, plastic hinge, shear-moment interaction, beam-column connection

1. Introduction

Many brittle fractures were observed in the beam-to-column connections of steel moment resisting frames (SMRFs) after the Northridge earthquake in 1994 and the Kobe earthquake in 1995 (Miller, 1998). In order to overcome this issue, some approaches have focused on increasing the stiffness of the connection, while others have focused on shifting the location of inelasticity away from the beam-column connection. In the latter case, the beam section can be intentionally weakened at a specific distance from the beam-column connection. As a result, plastic hinges will form within the reduced section of the beam away from the column's face. Intentional reduction can be introduced in the flanges of the beam, creating a reduced beam section (RBS), or reduction can be introduced in the web of the beam, creating a reduced web section (RWS). Extensive experimental studies confirm that RBS connections develop high inelastic deformations and sustain acceptable plastic rotations (Engelhardt *et al*., 1998; Chen, 2001; Jin and El-Tawil, 2005; Ricles *et al*., 2004; Itani *et al*., 2004). However, investigations about the RWS connections are still scattered and scarce. The results of limited analyses carried out by Kazemi and Hoseinzadeh Asl (2001) showed that the frames with RWS connections can provide at least the same level of seismic improvement as frames with RBS connections. Lepage *et al*. (2004) used the reduced web section beams in SMRFs, and the reduced zones of the beams were modeled using uncoupled rigid-plastic springs. Moreover, nonlinear behavior and ultimate capacity of plate girders utilizing circular or rectangular web openings were investigated by Shanmugan *et al*. (2002). It is important to note that utilizing RBS connections can cause a reduction in frame stiffness, and this reduction may lead to at least 4 percent increase in story drift ratio (Lee and Chung, 2007). However, introducing a perforation in the beam web does not have a significant effect on the lateral stiffness of the frame. Experimental studies have shown that seismic energy will be dissipated by local deformation in the perforated regions of the beams in the case of severe earthquake action. In these beams, the expected failure mode of a ductile frame, i.e., 'strong column but weak beam' and 'strong connection but weak component', will be reached, which will improve the seismic behavior of SMRFs (Qingshan *et al*., 2009). Previous investigations have demonstrated that RWS steel beams with various opening shapes and sizes behave similarly in terms of deformed shapes under a wide range of applied bending

Received August 14, 2014; accepted October 9, 2016;
published online June 30, 2017

*Corresponding author
Tel: +1-515-708-5797
E-mail: babakm@iastate.edu

moments and shear forces (Liu and Chung, 2003; Kazemi *et al*., 2012). Moreover, the failure modes are common among all beams, namely, shear failure, exural failure and Vierendeel mechanism, depending on the loading, the support conditions of the beams and the location of the web openings along the beam length. Furthermore, the load-deflection curves of RWS steel beams with different perforation shapes and sizes are also very similar to each other (Liu and Chung 2003; Kazemi *et al*., 2012). Experimental tests have shown that using L-shaped plates as stiffeners in the perforated area in RWS connections improves seismic performance of steel moment frames (Mirghaderi *et al*., 2013). In addition, Kazemi and Erfani (2007) proposed a shear-flexural mixed link element, called a VM link element that can be used for considering the interaction between the shear force and the flexural moment in reduced web beam connections. Additionally, in composite beams, several adjacent openings may lead to secondary deformations and *P*-Δ effect should be considered in these connections (Lawson *et al*., 2006). It is necessary to note that in circular perforations, a plastic hinge forms at the weakest region (middle) of the opening, while in rectangular and long enough elliptical shapes, plastic hinges form at two ends of the opening. Therefore, the latter shapes dissipate the seismic energy more efficiently (Hedayat and Celikag, 2009). Despite the fact that extensive studies have investigated about the RWS connections, there is a need for further study about the influence of the perforation on the performance of the moment connection and a need to develop a shear-flexural interaction formula for designing the connections, which is scarce in the current literature. Moreover, reliability of the design procedure needs to be assessed by designing and studying the behavior of a moment frame.

This paper presents a parametric study on the effect of perforation size, perforation location, and span length of RWS connections. In order to reduce the local buckling effect, a perimeter stiffener is used around the perforation. In addition, an interaction formula for bending moment and shear force is derived for design purposes. Furthermore, a step-by-step method for designing these connections is prescribed. Finally, the performance of an RWS frame is compared with the performance of a conventional frame under cyclic loading.

2. Verification of Finite Element Model

The experimental specimen, RBS1, shown in Fig. 1, tested by Pachoumis *et al*. (2009), was simulated in ABAQUS (Hibbitt *et al*., 2001) to verify the finite element (FE) model. A bilinear material was assigned to the members using Young's modulus E =207 GPa, yield stress f_y=305 Mpa and ultimate stress f_u=510 Mpa. A Nonlinear static analysis was performed on the simulated frame using the Full Newton method as the solution technique.

Tie interaction was utilized to connect the beam flanges and continuity plates to the column. All six degree of freedoms (DOFs) were restrained at both ends of the column to be in agreement with the experimental test setup. Cyclic loading shown in Fig. 2(a) was applied to the free end of the beam. A 4-node reduced integrated shell element was employed to mesh the members. Figure 2(b) shows that the FE model could successfully predict the behavior of the connection. Also, local deformation of the connection is in good agreement with the test results as shown in Fig. 3.

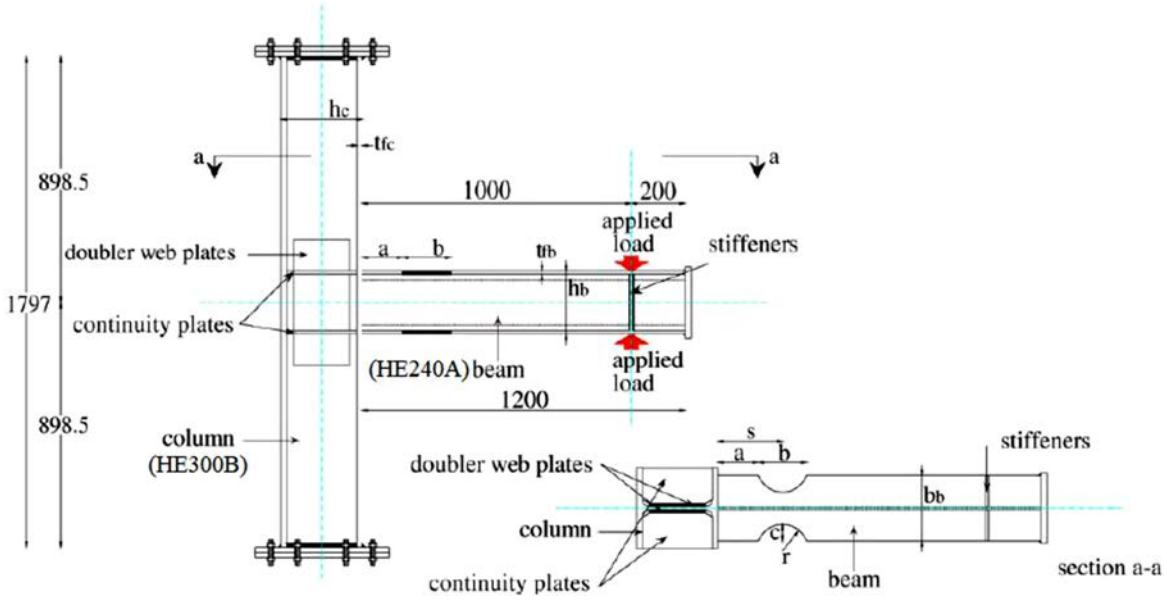

Figure 1. Test setup (Pachoumis *et al*., 2009).

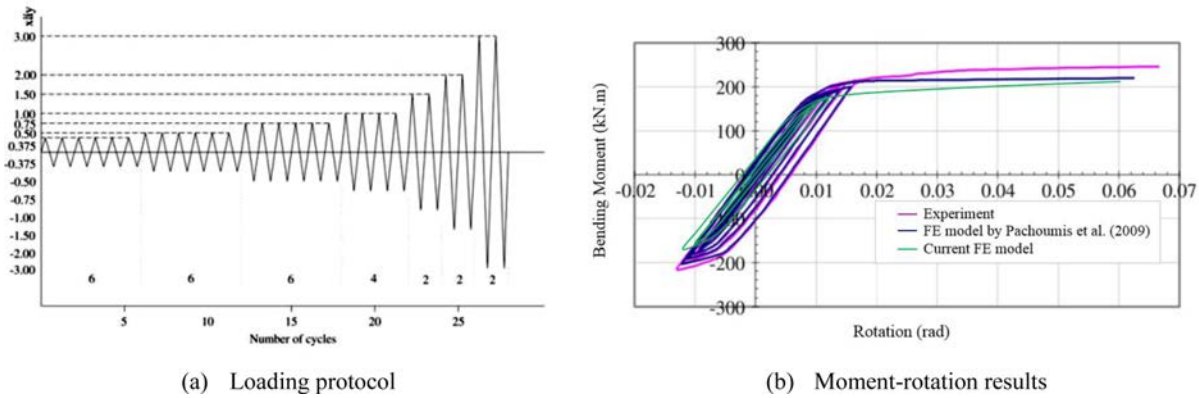

(a) Loading protocol (b) Moment-rotation results

Figure 2. Loading protocol and comparison of FE and experimental results (Pachoumis *et al*., 2009).

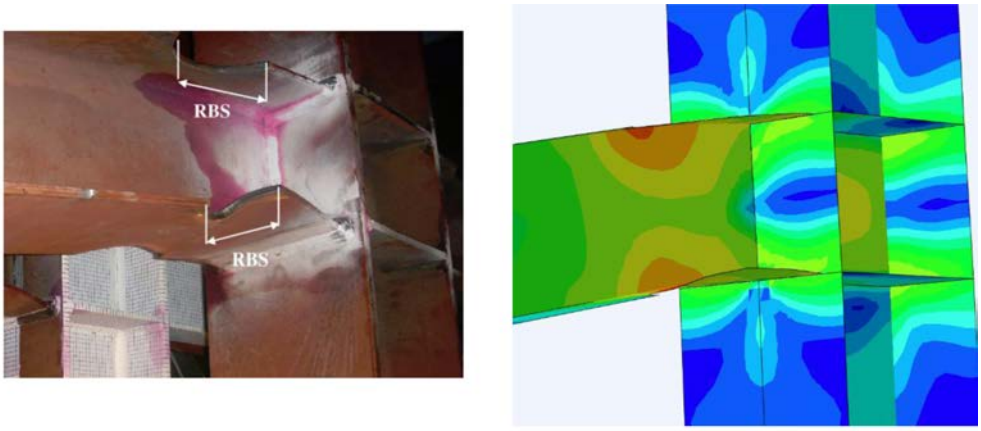

(a) Local deformation of connection in test (Pachoumis *et al*., 2009) (b) Simulation results

Figure 3. Comparison of experimental and simulation results.

3. Description of FE models

Eighteen models with different perforation sizes, perforation locations and span lengths were modeled in a general purpose FE software, ABAQUS (Hibbit *et al*., 2001). The configuration of the models is illustrated in Fig. 4. In order to avoid stress concentration, a circular fillet was applied to the corners of the perforations and a stiffener was tied to the edge of the perforation to prevent any local buckling. The stiffener dimensions were chosen based on the compactness criteria prescribed in Seismic Provision 2005 to prevent any local buckling in the perforated region. A bilinear stress-strain relationship was used for the material to account for the elastic and strain

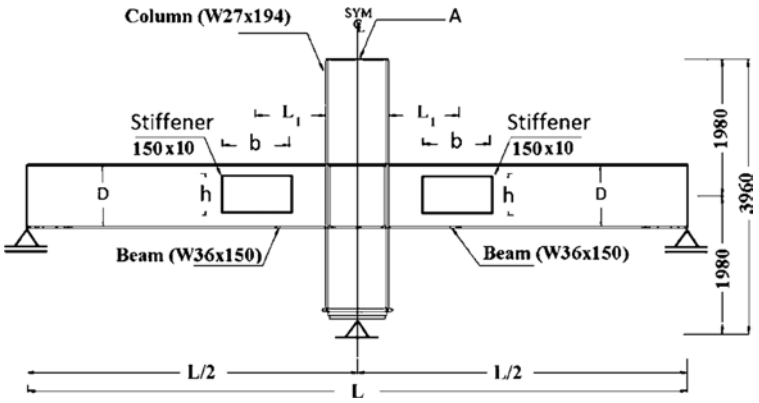

Figure 4. The RWS connection model (dimensions in mm).

hardening stages. The Young's modulus E=206 GPa, yielding stress f_y=235 MPa and ultimate stress f_u=363 MPa was used for the material. A nonlinear static general analysis was performed on the models using the Full Newton method as the solution technique. Similar to the verification model, beams and continuity plates are tied to the column to prevent any penetration between the members. Translational DOFs of the bottom of the column were restrained to simulate the pin support. Moreover, the free ends of the beams were restrained from vertical translation. Lateral monotonic displacement was applied to the top of the column (point A in Fig. 4). A 4-node reduced integrated element (S4R) was employed to mesh the members, and finer mesh was assigned in the vicinity of the perforation to successfully capture the local deformation of connection.

In Fig. 4:

D: Depth of the beam.

b: width of the perforation.

h: height of the perforation.

L_1: Distance between the middle of the perforation and face of the column.

Each model's ID represents the height, width and location of the perforation as shown in Fig. 5. It should be noted that there is an extra digit at the end of the last two models which show the length of each beam (L/2) in meters. The first digit, L_1, is designated as D or 0.75D. L_1 cannot be less than the latter case owing to the fact that the end of the perforation will be too close to the columns' face. On the other hand, it cannot be larger than D due to the fact that the perforation will be too far away from the connection and it will not affect the local behavior of the connection. The second digit (b/h) is designated as 1, 1.5 or 2. A square opening will be achieved by choosing the first shape factor, and it is recommended that the shape factor be limited to 2.5 (Lawson *et al*., 2006). In this study, shape factor is limited to 2 to be more conservative. The third digit (h/D) is designated as either 0.65, 0.75 or 0.85. The latter case shows the maximum possible perforation height without cutting the flanges and the first one shows the minimum h/D without negating the effect of the opening. Dimensions of the models are listed in Table 1.

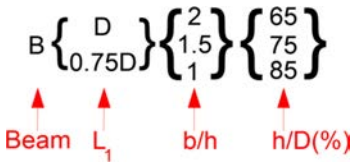

Figure 5. Definition of models' IDs.

4. FE Results

According to AISC Seismic Provisions (2005), in special moment frames, beam-to-column connections shall be capable of sustaining an inter-story drift angle of at least 0.04 radians. In order to achieve this purpose, the following three conditions must be satisfied at the target inter-story drift angle:

(a) The connection components at the face of the column must be designed to remain elastic, in the fully yielded and strain-hardened condition that can be forced in the reduced section, under seismic loads and gravity loads. This will satisfy 'strong connection but weak component' criteria;

Table 1. Models' dimensions

Models	h (mm)	b (mm)	b/h	h/D (%)	L_1 (mm)	L_1/D	L (mm)
BD285	780	1560	2	85.3	914.4	1	9000
BD275	690	1380	2	75.5	914.4	1	9000
BD265	600	1200	2	65.6	914.4	1	9000
BD1.585	780	1170	1.5	85.3	914.4	1	9000
BD1.575	690	1035	1.5	75.5	914.4	1	9000
BD1.565	600	900	1.5	65.6	914.4	1	9000
BD185	780	780	1	85.3	914.4	1	9000
BD175	690	690	1	75.5	914.4	1	9000
BD165	600	600	1	65.6	914.4	1	9000
B0.75D265	600	1200	2	65.6	685.8	0.75	9000
B0.75D1.585	780	1170	1.5	85.3	685.8	0.75	9000
B0.75D1.575	690	1035	1.5	75.5	685.8	0.75	9000
B0.75D1.565	600	900	1.5	65.6	685.8	0.75	9000
B0.75D185	780	780	1	85.3	685.8	0.75	9000
B0.75D175	690	690	1	75.5	685.8	0.75	9000
B0.75D165	600	600	1	65.6	685.8	0.75	9000
BD2853	780	1560	2	85.3	914.4	1	6000
BD2856	780	1560	2	85.3	914.4	1	12000

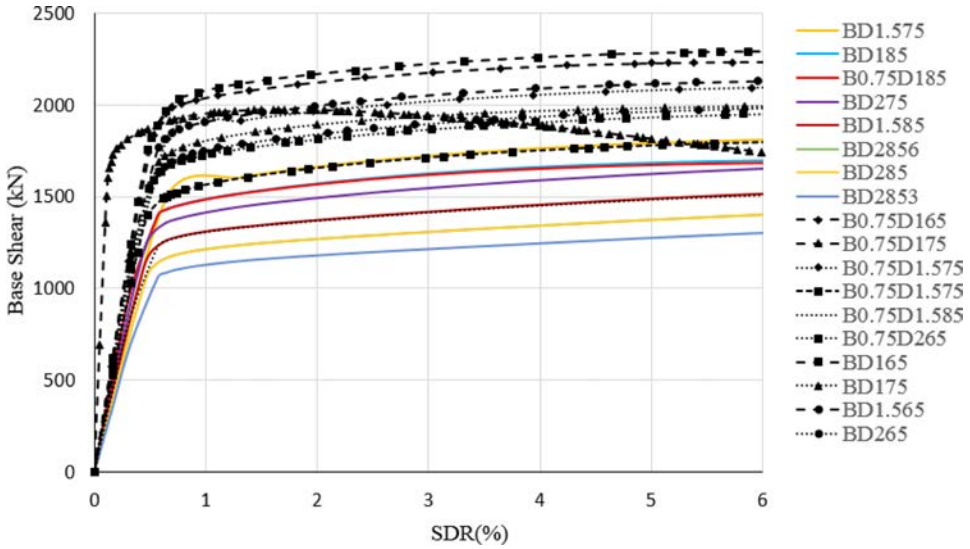

Figure 6. Base Shear vs. SDR.

Table 2. Acceptability of each model

Models	Yielding at column's face	Peak plastic strain around perforation	Strength degradation (%)	Acceptability
BD285	No	0.16	No	Yes
BD275	No	0.14	No	Yes
BD265	Yes	0.12	No	No
BD1.585	No	0.15	No	Yes
BD1.575	No	0.19	No	Yes
BD1.565	Yes	0.08	No	No
BD185	No	0.14	No	Yes
BD175	Yes	0.14	No	No
BD165	Yes	0.1	No	No
B0.75D265	Yes	0.1	No	No
B0.75D1.585	Yes	0.08	No	No
B0.75D1.575	Yes	0.1	No	No
B0.75D1.565	Yes	0.11	No	No
B0.75D185	No	0.16	No	Yes
B0.75D175	Yes	0.13	5.0	No
B0.75D165	Yes	0.1	No	No
BD2853	No	0.14	No	Yes
BD2856	No	0.14	No	Yes

(b) In order to avoid any fracture in the reduced section, maximum plastic strain shall be less than the ultimate strain of steel, which is assumed to be 0.2;

(c) Strength degradation in the connections should be less than 20%.

The models are pushed to 6% story drift ratio (SDR) and the results of the analyses are shown in Fig. 6. The models that do not fulfill the above conditions are shown in dashed black curves in this figure. SDR can be calculated by dividing the displacement at point A by the height of the column. Among the acceptable models, BD1.575 has the largest and BD2853 has the smallest base shear capacity. In addition, in Table 2, each model is evaluated based on the aforementioned provisions. Although peak plastic strain is less than the ultimate strain in all the models, some of the cases are not acceptable owing to the development of the plastic strain in the beam flanges at the face of the columns. For instance, Fig. 8 shows the plastic strain development in the beam flange at the column's face in BD165 model. The selected elements of this model is shown in Fig. 7.

Based on the results, following conclusions can be drawn:

• Most of the cases with a square-shaped perforation ($b/h=1$) failed to satisfy the aforementioned provisions as shown in Table 2. In these cases, the beam did not remain

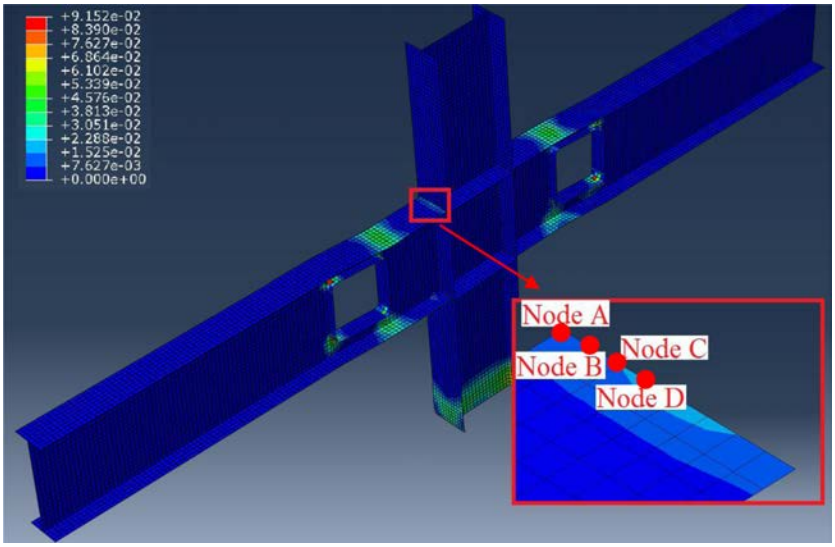

Figure 7. Selected elements in beam flange at column's face in BD165 model.

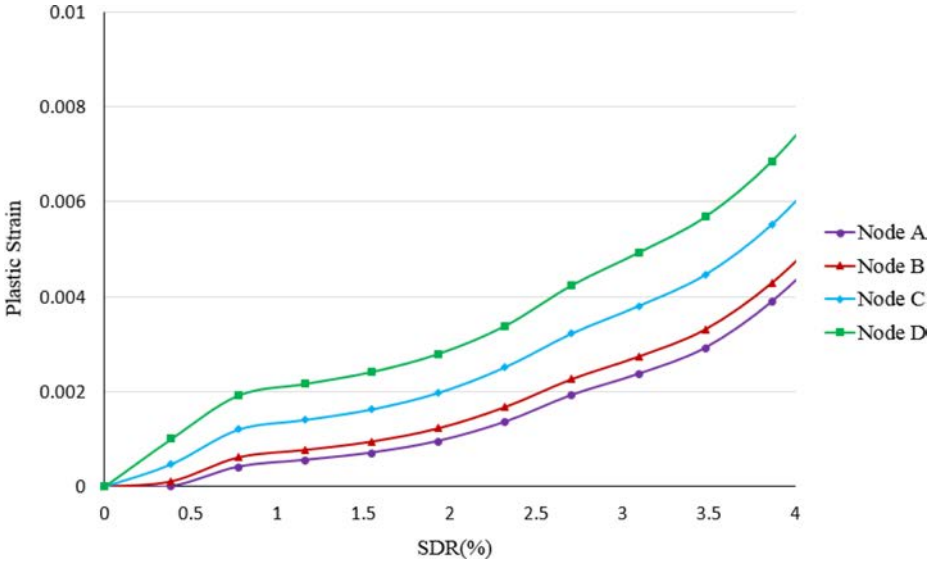

Figure 8. Development of plastic strain vs SDR in the selected elements in in BD165 model.

elastic at the face of the column. As an example, plastic strain development in one of these cases is shown in Fig. 7. On the other hand, using a long opening ($b/h>2$) leads to larger plastic strain in the perforation area due to the P-Δ effect (Lawson, *et al*. 2006). Thus, width of the perforation can be chosen based on Eq. (1).

$$h < b < 2h \tag{1}$$

• Comparison of the models with the same perforation width demonstrates that when h/D is equal to 65%, beams do not remain elastic at the face of column. Thus, the perforation is too small to satisfy the predefined requirements. On the other hand, when h/D is equal to 85%, the capacity of the cases decrease substantially. As it can be seen in Fig. 6, at the 4% SDR, the base shear capacity of the model BD285 is 20% less than BD275. Therefore, it is better to have the height of the perforation be less than 0.85D as it is shown in Eq. (2).

$$0.65D < h < 0.85D \tag{2}$$

• In almost all the cases that L_1 was equal to $0.75D$, plastic strain was observed at the face of the column, which is not acceptable. This is mainly owing to the fact that the perforation end was too close to the column face, thus the plastic strain around the opening propagated to the elements located at the face of the column. Thus, L_1 should be made larger than D.

5. Cyclic Analysis

In order to assess the behavior of RWS connections under cyclic loading, static cyclic analyses were carried

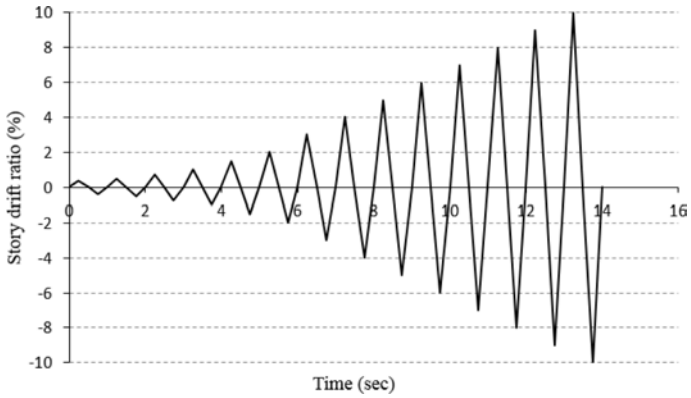

Figure 9. Cyclic displacement applied to models.

out on the acceptable models identified in the previous section. Lateral cyclic displacement shown in Fig. 9 was applied at point A (Fig. 4) of the column. Boundary conditions, interactions and other modeling parameters are identical with pushover cases.

Figure 10 shows the hysteretic response of the eight accepted models. As can be seen in this figure, stable hysteretic behavior is observed in all models, and they reached 4% SDR without strength degradation. Also, this fact can be seen in as well. In this figure, V represents the absolute value of the peak base shear in different SDRs. Based on Fig. 11, it can be concluded that strength loss in all cases started after 5% SDR, and around 7-8% SDR, they lost more than 20% of their strength. It should be noted that the cases will reach the collapse SDR if peak plastic strain in the models does not exceed 0.2 prior to this SDR.

6. Interaction Formula

The deformation of a moment frame under lateral forces is presented in Fig. 12. In this frame, beams can be simplified to a cantilever beam owing to the zero bending moment in the mid-span of the beams. Therefore, shear force and bending moment in the middle of the perforation can be calculated as shown in Fig. 12.

Shear and bending moment interaction in RWS connections is of great importance for design purposes. Cantilever beams shown in Fig. 12 are modeled in ABAQUS to derive an interaction formula for RWS connections. Dimensions of the opening in the simulated beams are identical with the accepted models in the previous sections. Results of the analyses in previous sections demonstrate that inelastic behavior of the beams is concentrated around the perforation and the middle portions of the beams are elastic (Fig. 8). Therefore, lengths of the studied beams were assumed to be equal to $2L_1$ and the elastic part is eliminated from the simulation. A combination of shear and moment forces were applied to the end of the beams. The flexural-shear force interaction curve for each model is shown in Fig. 13. In this figure, the M_p and V_p are plastic moment and plastic shear strength of the beam, respectively, while M and V are applied moment and shear force on the beam in combined loading, respectively.

An interaction formula is derived for each model based on the fitted curves as shown in Fig. 13. Considering all the curves in this figure, two boundary curves can be derived: the lower and upper bound curves which have the smallest and largest enclosed area, respectively. The interaction formula for each bound is shown in Eqs. (3) and (4).

$$\left(\frac{V}{V_p}\right)^{2.5}+\left(\frac{M}{M_p}\right)^{1.2}=1 \quad \text{lower bound} \tag{3}$$

$$\left(\frac{V}{V_p}\right)^{2.5}+\left(\frac{M}{M_p}\right)^{2.5}=1 \quad \text{upper bound} \tag{4}$$

In these equations, V, M, V_p, and M_p are applied shear force, bending moment, plastic shear and plastic moment at the perforated section, respectively. The lower bound equation can conservatively be used for the beam section design and the upper bound equation can conservatively be used for the design of the connection.

7. Design Procedure

The design procedure is described in the following steps, so that the connection components outside the opening remain elastic in the fully yielded and strain-hardened condition that can be forced in the reduced section, under seismic loads and gravity loads:

1-Calculation of V_{RWS} and M_{RWS}

Figure 14 shows the shear force at the center of the reduced section. The maximum shear and moment at each T section is equal to $V_{RWS}/2$ and $V_{RWS}b/4$, respectively. A shear-flexural interaction can be written for the mentioned section as follows:

$$\left(\frac{\frac{V_{RWS}}{2}}{R_yC_{pr}(0.6F_y)A_w}\right)^2+\left(\frac{\frac{V_{RWS}b}{4}}{R_yC_{pr}F_yZ_{RWS-T}}\right)^2=1 \tag{5}$$

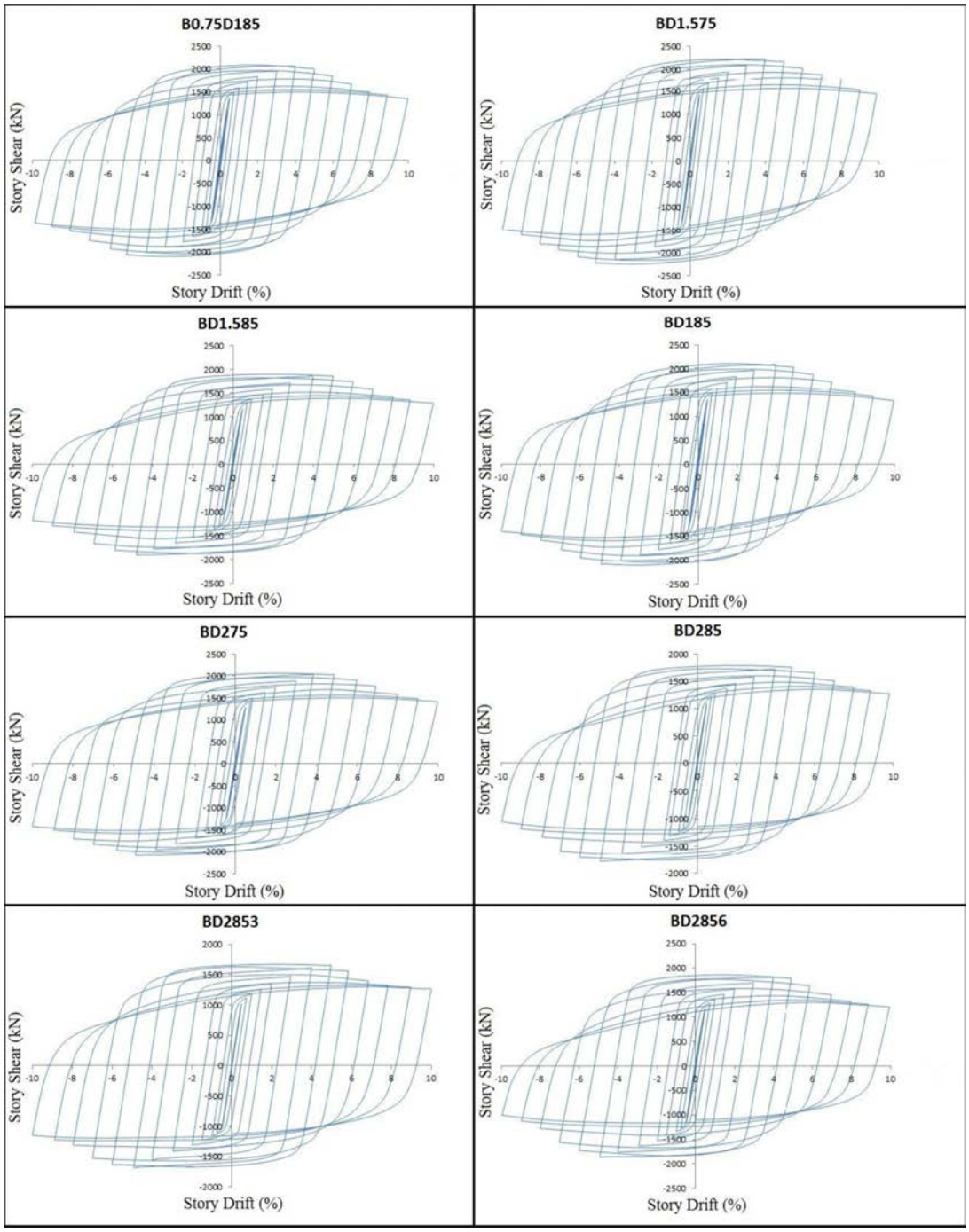

Figure 10. Hysteresis response of models.

By simplifying the above equation, the V_{RWS} can be easily calculated. In the above equation, R_y is the ratio of the expected yield stress to the specified minimum yield stress and is taken as 1.1, as suggested by AISC Seismic Provisions (2005). C_{pr} is the factor to account for peak connection strength, including strain hardening, and is equal to 1.15 as prescribed in AISC Prequalified Connections (2005). A_w is the total web area of a single T section and $Z_{RWS\text{-}T}$ is the plastic section modulus of a single T section of the reduced section including stiffener. b is the perforation length as illustrated in Fig. 4. Also, the maximum flexural strength at the center of the reduced web section, M_{RWS}, can be calculated as:

$$M_{RWS} = R_y C_{pr} Z_{RWS} F_y$$

where Z_{RWS} is the total plastic section modulus of the reduced section.

2-Calculation of V_L, V_R, M_L, and M_R

The expected shear force and flexural moment at the

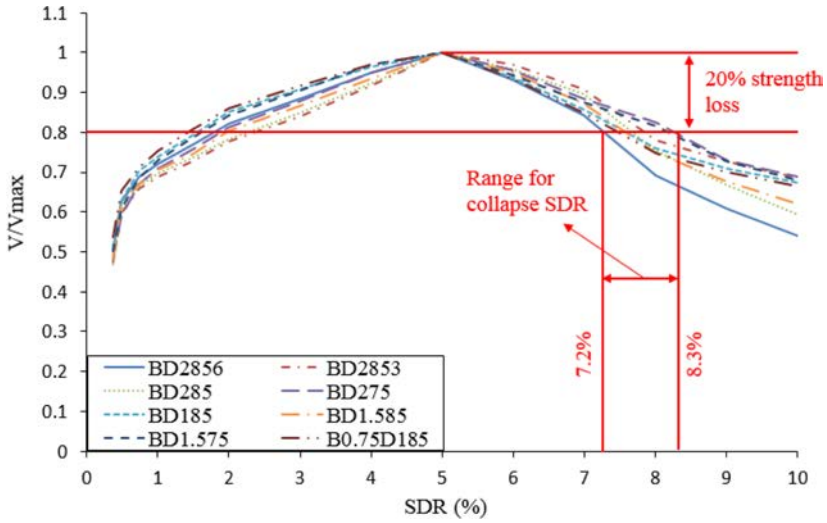

Figure 11. Base shear ratio vs. SDR.

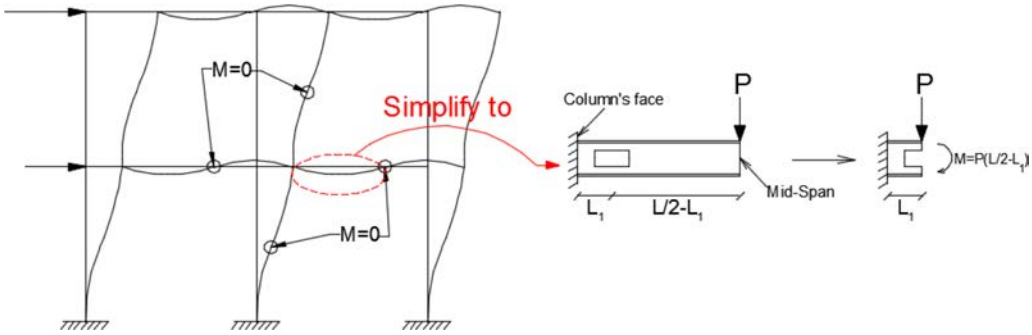

Figure 12. Effect of the beam length on the bending moment at reduced section.

left side (V_L and M_L) and the right side (V_R and M_R) of a beam are shown in Fig. 15. Moreover, $M_{f\text{-}left}$ and $M_{f\text{-}right}$ are bending moment at the face of the left and right columns, respectively. Also, q represents the uniform gravity load applied to the beam.

By solving the Eqs. (7) to (10), V_L, V_R, M_L, and M_R can be obtained:

$$\left(\frac{V_L}{V_{RWS}}\right)^{2.5}+\left(\frac{M_L}{M_{RWS}}\right)^{1.2}=1 \tag{7}$$

$$\left(\frac{V_R}{V_{RWS}}\right)^{2.5}+\left(\frac{M_R}{M_{RWS}}\right)^{1.2}=1 \tag{8}$$

$$V_L=\frac{M_R+M_L}{L_h}+\frac{qL_h}{2} \tag{9}$$

$$V_R=\frac{M_R+M_L}{L_h}+\frac{qL_h}{2} \tag{10}$$

The first two above equations are interaction equations in the reduced section. The others are static equations for the middle part of the beam in Fig. 15.

3-Calculation of $M_{f\text{-}Left}$ and $M_{f\text{-}Right}$

Expected moment at the face of the column can be calculated by Eqns. 11 and 12:

$$M_{f-Left}=M_L+V_LL_1+q\frac{L_1^2}{2} \tag{11}$$

$$M_{f-Right}=M_R+V_RL_1+q\frac{L_1^2}{2} \tag{12}$$

4-The $M_{f\text{-}Left}$ and $M_{f\text{-}Right}$ of Eqs. (11) and (12) must be less than the flexural strength of the ends of the girder, φM_n:

$$M_{f-Left}\le\varphi M_n \tag{13}$$

$$M_{f-Right}\le\varphi M_n \tag{14}$$

8. Frame Analysis

In order to assess the reliability of the developed design method, the frames shown in Fig. 16 are simulated in ABAQUS. Story height, member sections and span lengths are presented in Fig. 16. Material, mesh type, and interactions

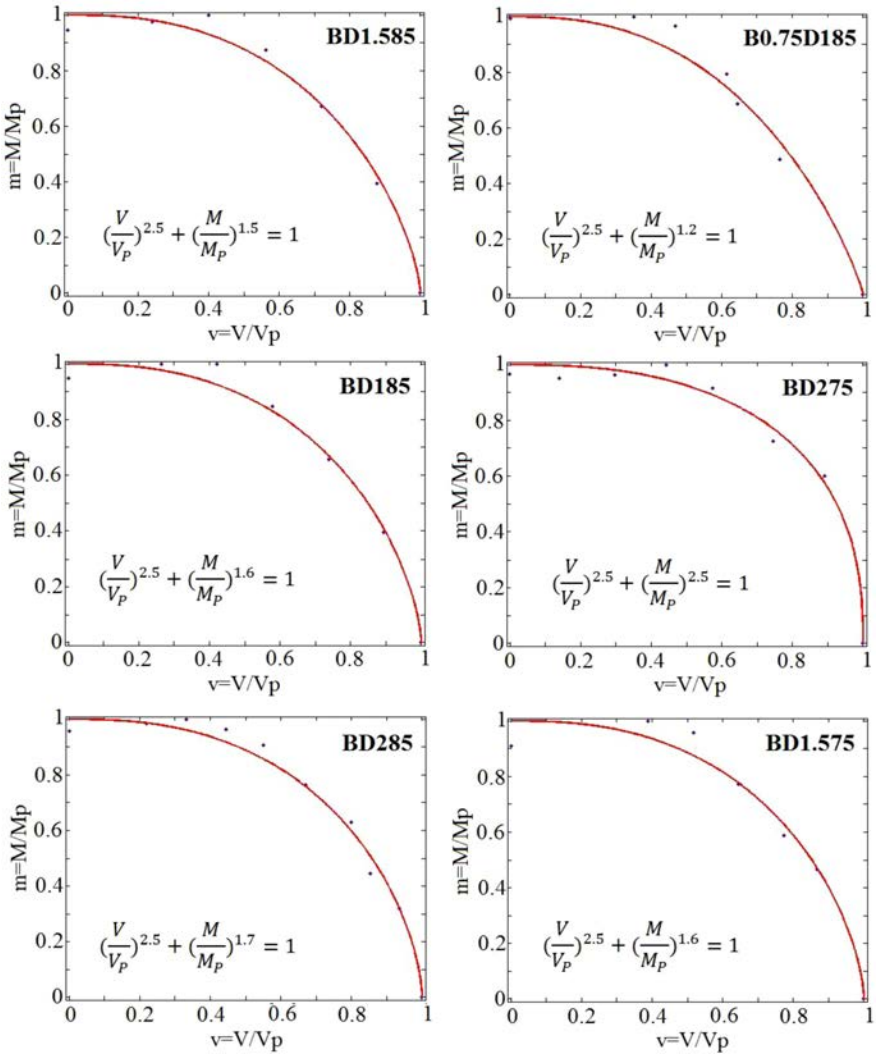

Figure 13. Flexural-shear force interaction of beams with perforation.

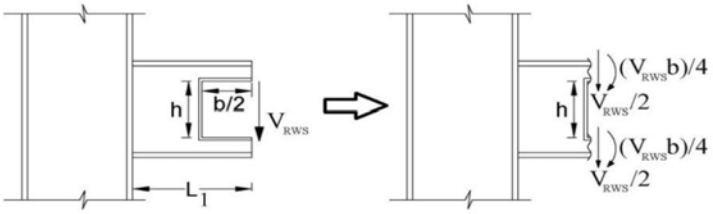

Figure 14. Bending moment and shear force at each T section.

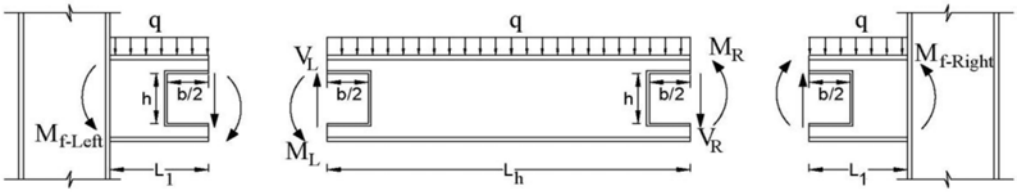

Figure 15. Structural layout of expected forces in the beam.

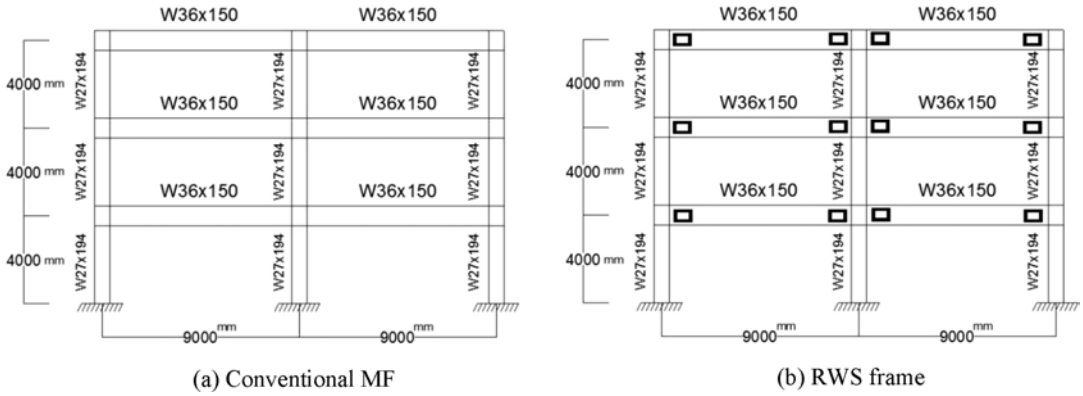

Figure 16. Modeled frames.

Table 3. Dimensions of the openings

h (mm)	b (mm)	b/h	h/D (%)	L_1 (mm)	L_1/D
690	1035	1.5	75.5	914.4	1

are similar to those used in cyclic analyses. A nonlinear static general analysis was performed on each frame, and the Full Newton method was used as the solution technique. It is assumed that the simulated frames are perimeter frames to which the gravity load does not apply, and only resist lateral seismic loads. In the conventional moment frame the beams do not have any openings in the web, while in the RWS frame (RWSF), a perforation is introduced in the beams. Openings' dimensions are determined based on the design procedure of section 5 and are illustrated in Table 3.

Utilizing Eqs. (5) and (6), V_{RWS} and M_{RWS} are equal to 241 and 2631 kN·m, respectively. By solving the Eqs. (7) to (10), and considering the fact that there is no gravity load, M_L, M_R, V_L, and V_R can be calculated as 778, 778 kN·m, 217 and 217 kN, respectively. Finally, according to Eqs. (11) and (12), the bending moments at the face of the columns are equal to 975 kN·m, which are less than φM_n =2056 kN·m and the Eqs. (13) and (14) are fulfilled.

Figure 17 shows the lateral displacement protocol which is applied to the roof in the simulated frames.

Base shear versus overall drift ratio of simulated frames are compared in Fig. 18. As can be seen in this figure, the peak strength of RWSF is less than the conventional frame, which is mainly due to introducing the openings in the beams. Also, it can be observed that the RWS frame successfully reached 4% overall drift ratio without any strength degradation. Overall drift ratio (ODR) can be calculated by dividing the roof displacement by the frame height. It is noteworthy that plastic strain in the roof of the conventional frame reached the fracture point around 2% ODR, and at 4% ODR, plastic strain developed beyond the fracture point in all three stories. However, plastic strain did not reach the fracture limit until around 4% ODR in RWSF, and it occurred in the vicinity of the perforations. Plastic strain distribution in the frames is presented in Fig. 19. In this figure, blue, red and grey elements represent the elastic, inelastic, and fractured elements, respectively. Results of the analysis of the conventional frame showed that plastic strains started to develop in the middle column at the second story and then other connections started to yield. However, in the RWS frame (RWSF) all the connections remained elastic at 4% ODR and plastic strains developed in the vicinity of the weakened area except for the third story. The

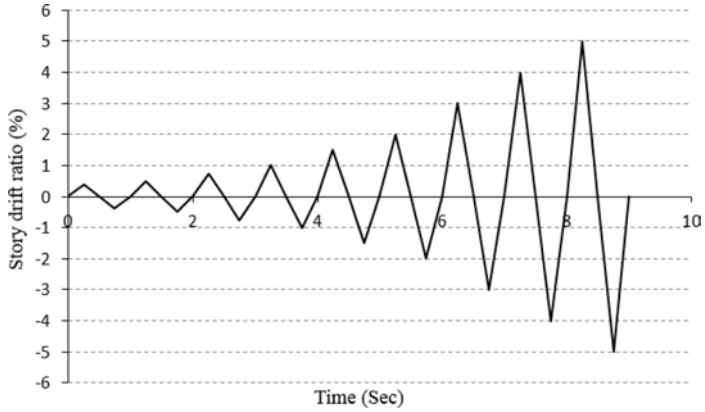

Figure 17. Loading protocol applied to the frames.

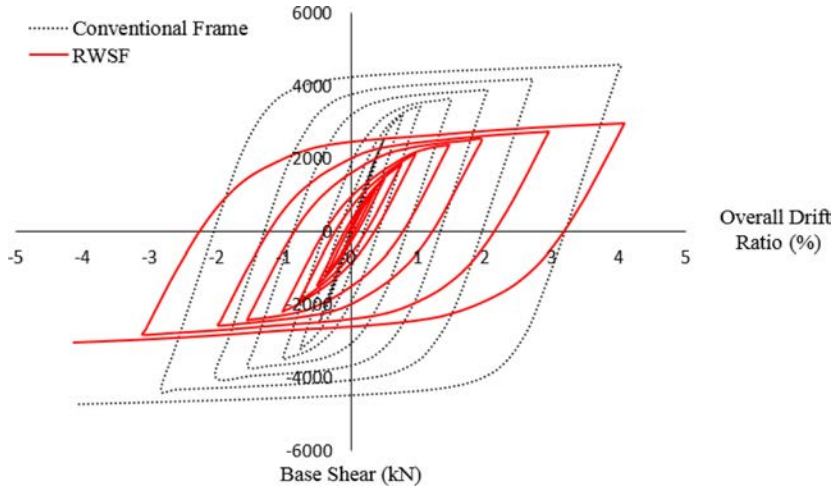

Figure 18. Base shear vs. ODR in the simulated frames.

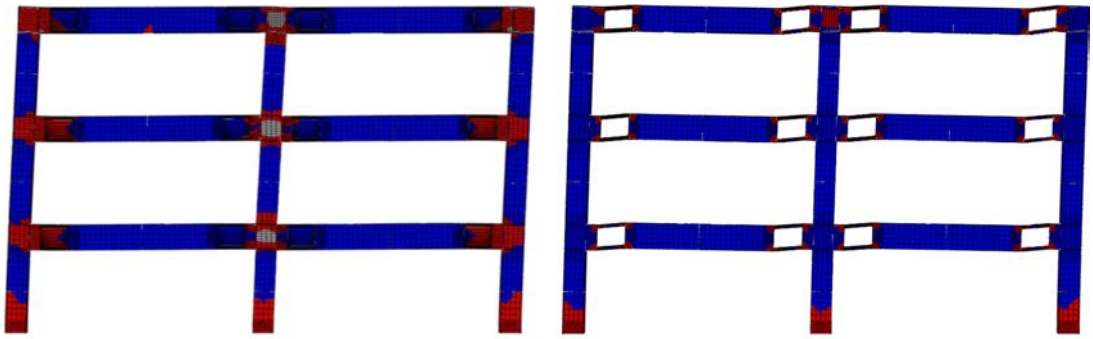

Figure 19. Plastic strain distribution in the simulated frame.

bending moments transferred by the connections of the third story were sustained by one column at each connection, while in the other stories, two columns sustained the moment in the connection; thus it is expected that plastic strains at the third story of RWSF would develop in the connection. Therefore, it is more economical to use conventional beams in the roof of RWSFs. Based on the results, it can be concluded that RWS connections can effectively improve the behavior of SMFs and plastic strain will be successfully shifted from the connections to the perforated region.

9. Conclusion

Investigations were carried out on seismic behavior of steel moment frames with RWS connections, which includes a perforation at the beam's web just away from the column's face. Eighteen finite element models were analyzed and a parametric study was done on the effect of the perforation size, location and beam span length of RWS connections. Then, a step-by-step design procedure was developed and a special moment frame was designed based on the developed design procedure. The main concern was whether or not the RWS connections can improve the behavior of the conventional special moment frames. Major conclusions of this study are drawn as follows:

(1) Perforation height should be chosen between 65% and 85% of the height of the beam to satisfy the seismic demands. Lower values will result in developing plastic strain in the beam at the column's face, which is not desired. On the other hand, the upper bound causes significant strength degradation in the reduced section which is not acceptable.

(2) Width over height of the perforation (shape factor) should be larger than one and less than two.

(3) Distance between the middle of the perforated section and the face of the column should be at least equal to the height of the beam.

(4) Strength degradation in RWS connections begins after 5% story drift ratio. Therefore, the connections can successfully sustain 4% story drift ratio, which is required by current design code.

(5) Flexural strength is affected by shear force in connections with web openings, therefore, an interaction formula between shear and bending moment is developed.

(6) RWS connections can effectively improve the

behavior of conventional special moment frames, and plastic strains will be shifted from the panel zone to the perforated region.

References

AISC (2005). Prequalified Connections for Special and Intermediate Steel Moment Frames for Seismic Applications. American Institute of Steel Construction. Chicago, Illinois.

AISC (2005). Seismic Provisions for Structural Steel Buildings. American Institute of Steel Construction. Chicago, Illinois.

Chen, S.J. (2001). "Design of ductile seismic moment connections, increased beam section method and reduced beam section method." *International Journal of steel structures,* 1, pp. 45-52.

Engelhardt, M.D., Winneberger, T, Zekany, A.J., and Potyraj, T.J. (1998). "Experimental investigation of dogbone moment connections." *Engineering Journal of AISC*, 35, pp. 128-139.

Hibbitt, Karlsson, and Sorensen (2010). "ABAQUS/ Standard user's manual: Hibbitt, Karlsson & Sorensen".

Hedayat, A.A. and Celikag, M. (2009). "Post-Northridge connection with modified beam end configuration to enhance strength and ductility." *Journal of Constructional Steel Research,* 65, pp. 1413-1430.

Itani, A.M., Cheng, Z., and Saiidi, M. (2004). "Cyclic response of steel moment connections for large beam sections using haunch and reduced beam section concepts." *International Journal of steel structures*, 4, pp. 147-155.

Jin, J and El-Tawil, S. (2005). "Seismic performance of steel frames with reduced beam section connections." *Journal of Constructional Steel Research*, 61, pp. 453-471.

Kazemi, M.T. and Erfani, S. (2007). "Analytical study of special girder moment frames using a mixed shear-flexural link element." *Canadian Journal of Civil Engineering,* 34, pp. 1119-1130.

Kazemi, M.T. and Hoseinzadehasl, M. (2001). "Modeling of inelastic mixed hinge and its application in analysis of the frames with reduced beam section." *International Journal of Steel Structures*, 11, pp. 51-63.

Kazemi, M.T., Momenzadeh, S., and Hoseinzadehasl, M. (2012). "Study of Reduced Beam Section Connections with Web Opening." *15th World Conference on Earthquake Engineering*, Lisbon, September.

Lawson, R.M., Lim, J, Hicks, S.J., and Simms, W.I. (2006). "Design of composite asymmetric cellular beams and beams with large web openings." *Journal of Constructional Steel Research,* 62, pp. 614-629.

Lee, C.H. and Chung, S.W. (2007). "A simplified analytical story drift evaluation of steel moment frames with radius-cut reduced beam section." *Journal of Constructional Steel Research,* 63, pp. 564-570.

Lepage, A., Aschheim, M., and Senescu, R. (2004). "Shear-yielding steel outriggers for high-rise construction." *Proc.13th World Conference on Earthquake Engineering,* Canadian association of earthquake engineering, Vancouver, B.C. paper 2078.

Liu, T.C.H. and Chung, K.F. (2003). "Steel beams with large web openings of various shapes and sizes: finite element investigation." *Journal of Constructional Steel Research*, 59, pp. 1159-1176.

Miller, D.K. (1998). "Lessons learned from Northridge earthquake." *Engineering Structures,* 20, pp. 249-260.

Mirghaderi, S.R., Shahabeddin, T., and Imanpour, A. (2010). "Seismic performance of the accordion-web RBS connection." *Journal of Constructional Steel Research*, 66, pp. 277-288.

Qingshan, Y., Bo, L., and Na, Y. (2009). "Aseismic behaviors of steel moment resisting frames with opening in beam web." *Journal of Constructional Steel Research*, 65, pp. 1323-1336.

Pachoumis, D.T., Galoussis, E.G., Kalfas, C.N., and Christitsas, A.D. (2009). "Reduced Beam Section Moment Connections Subjected to Cyclic Loading: Experimental Analysis and FEM Simulation." *Engineering Structures*, 31, pp. 216-223.

Ricles, J., Zhang, X., Lu, L.W., and Fisher J. (2004). "Development of Seismic Guidelines for Deep-Column Steel Moment Connections." ATLSS Report No. *04-13*, ATLSS Engineering Research Center, Lehigh University, Bethlehem, PA.

Shanmugan, N.E., Lian, V.T., and Thevendran, V. (2002). "Finite element modelling of plate girders with web openings." Thin walled structures, 40, pp. 443-464.